ACS Sustainable Chemistry & Engineering

Research Article

pubs.acs.org/journal/ascecg

Simple Aqueous Preparation of High Activity and Stability NiFe Hydrous Oxide Catalysts for Water Oxidation

Chao Wang,[†,§] Reza B. Moghaddam,[†,‡,§] Michael J. Brett,[‡] and Steven H. Bergens*[,†]

[†]Department of Chemistry, University of Alberta, 11227 Saskatchewan Drive, Edmonton, Alberta T6G 2G2, Canada

[‡]Department of Electrical and Computer Engineering, University of Alberta, 9211 116 Street NW Edmonton, Alberta T6G 2V4, Canada

Supporting Information

ABSTRACT: A series of $Ni_{1-x}Fe_x$ hydrous oxide nanoparticles (HO-nps, x = 0−0.5, 1) were prepared by stirring 0.1 M KOH solutions of $NiCl_2$ and $FeCl_2$ under air at room temperature. The resulting HO-nps can be used directly, or washed and isolated without loss of activity. The $Ni_{1-x}Fe_x$ HO-nps are outstandingly active and stable toward the water oxidation reaction (WOR) in base. The $Ni_{0.75}Fe_{0.25}$ HO-np was the most active mass-normalized WOR catalyst in the series, with onset overpotential = 190 mV, Tafel slope = 24 mV dec^{-1}, overpotential at 10 mA cm^{-2} = 234 mV, and loadings Ni + Fe = 0.135 mg cm^{-2}. The catalysts were robust under long-term galvanostatic and duty-cycle testing. The $Ni_{0.75}Fe_{0.25}$ HO-np catalyst has a layered double hydroxide structure, and it appears that Fe enhances the activity of Ni toward the WOR by decreasing its electron density.

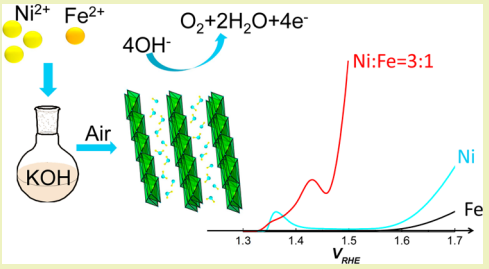

KEYWORDS: *Water electrolyzer, Water oxidation, Nickel, Iron, Alkaline electrolysis*

INTRODUCTION

We report a simple synthesis of active, stable catalysts for the water oxidation reaction (WOR) from common earth-abundant precursors. The large-scale electrolysis of water is a promising method to store energy from solar, wind, and other CO_2-free sources of electricity.[1,2] The resulting hydrogen can be combusted or converted into electricity with fuel cells.[3,4] Alternatively, carbon dioxide (CO_2) can be reduced at the electrolyzer cathode to form carbon monoxide or liquid fuels.[5] Alkaline water electrolyzers possess advantages over acidic systems.[6,7] Among the most significant is that non-noble metals catalyze the WOR in base.[8−10] The major challenge to the widespread adoption of electrolyzers for energy storage, however, is the sluggish WOR at the anode (eq 1, $E°$ = 1.23 V_{RHE}, RHE = reversible hydrogen electrode).[11,12]

$$4OH^- \rightarrow O_2 + 4e^- + 2H_2O \quad (1)$$

There are numerous reports of combinations of the first row metals Ni, Fe, Co, and Cu that are promising alkaline WOR catalysts.[13−22] Table 1 describes the most active in the literature. Most contain Ni and Fe. The active forms of these catalysts are hydrous oxides prepared by procedures including photochemical decomposition followed by heat treatment (Table 1, entry 1),[16] controlled electrodeposition followed by oxidation (entries 2 and 3),[23,24] or hydro/solvothermal treatment followed by modification with graphene oxide (GO) (entry 4)[25] or carbon nanotubes (CNTs) (entry 5).[14] Active FeCoW catalysts have very recently been prepared by careful hydrolysis, sol−gel formation, and drying with supercritical CO_2 (entry 6).[26]

Ideally, an industrial catalyst synthesis is inexpensive, simple, quick, and scalable.[6,20] We recently reported that $Ir_{1-x}Ni_x$ hydrous oxide nanoparticles (HO-nps) form as colloidal suspensions by stirring solutions of $NiCl_2$ and $IrCl_3$ in 0.1 M KOH under air for 3 days.[27] The resulting blue-purple colloids are active and stable WOR catalysts in acid. For this study, we report the preparation and study of a series of $Ni_{1-x}Fe_x$ HO-nps prepared in a similar manner for the WOR in base.

EXPERIMENTAL SECTION

Perchloric acid (Aldrich; 70%, 99.999%), potassium hydroxide (Aldrich; semiconductor grade, 99.99%), nickel chloride (Alfa Aesar; anhydrous, 98%), nickel chloride hydrate ($NiCl_2·6H_2O$; Baker; 98%), iron(II) chloride ($FeCl_2·4H_2O$; Fisher), iron(III) chloride ($FeCl_3·6H_2O$; Fisher), Ni foam (Goodfellow; thickness 1.6 mm; porosity 95%), Toray carbon fiber paper (Electrochem. Inc.), and Nafion (5 wt %, ElectroChem Inc.) were used as received unless stated otherwise. Triply distilled water was used throughout the experiments.

To prepare $Ni_{0.75}Fe_{0.25}$ HO-nps, 0.0259 g (0.20 mmol) of $NiCl_2$ or 0.0476 g (0.20 mmol) of $NiCl_2·6H_2O$ and 0.0133 g (0.067 mmol) of $FeCl_2·4H_2O$ or 0.0180 g (0.067 mmol) of $FeCl_3·6H_2O$ were dissolved in 20.0 mL of triply distilled water in a 100 mL round-bottom flask. A 3.0 mL portion of 0.83 M KOH solution was then added dropwise over 2 min. Upon adding KOH, the color of the solution changed from transparent pale green to dark green, with green particles. The color of the suspension then changed from green to yellow within 0.5 h, and the solution was stirred at 400 rpm for a total of 24 h in air. The use of $FeCl_3·6H_2O$ gave similar water oxidation activity and stability to

Received: October 4, 2016
Revised: October 25, 2016
Published: October 27, 2016

Downloaded via UNIV OF ALBERTA on July 4, 2018 at 16:53:20 (UTC).
See https://pubs.acs.org/sharingguidelines for options on how to legitimately share published articles.

© 2016 American Chemical Society

DOI: 10.1021/acssuschemeng.6b02391
ACS Sustainable Chem. Eng. 2017, 5, 1106−1112

Table 1. Reported Active Water Oxidation Catalysts in Base[a]

	catalyst	η_{onset} /V	η at 10 mA cm^{-2}/V (LSV)	Tafel slope (mV dec^{-1})	loading (mg cm^{-2})
1	Fe−Co[16]	0.18	NA	31	NA
2	NiFe/Pt foil[23]	NA	NA	14.8	NA
3	NiFe−LDH array/Ni foam[24]	0.20	0.23	52.8	1.0
4	FeNi−rGO LDH hybrid[25]	0.19	0.21	39	0.25
5	NiFe LDH−CNT hybrid[14]	0.22	0.25	31	0.25
6	FeCoW/Au plated Ni_{foam}[26]	NA	0.19	NA	0.39
	this work	0.19	0.23	24	0.135

[a]The following abbreviations apply: NA, not available; η, overpotential; LDH, layered double hydroxide; rGO, reduced graphene oxide.

$FeCl_2{\cdot}4H_2O$ (Figures S15 and S16). For the synthesis of other $Ni_{1-x}Fe_x$ HO-nps, appropriate masses of the metal precursors (i.e., $NiCl_2$ and $FeCl_2$) and 0.83 M KOH solution (10 equiv the total mole of Ni^{2+} and Fe^{2+}) were utilized to yield the desired metal ratios. Table S1 provides details of the chemicals used for the synthesis. The amount of Ni precursor was kept constant, and the amount of Fe was set to the desired mass. The $Ni_{1-x}Fe_x$ HO-nps can be stored in the reaction mixture, or washed and isolated as described in the Supporting Information.

The as-prepared colloidal Ni, Fe, and $Ni_{1-x}Fe_x$ HO-np solutions were mixed with appropriate amounts of Nafion to give a final 1% wt Nafion per total mass of Ni + Fe, calculated from the amounts in Table S1. Using a micropipette and graded microtips, appropriate volumes of the HO-np/Nafion suspensions (sonicated for 2 min) were drop coated onto ∼1 cm^2 area of carbon fiber paper electrodes (CF; 1 × 3 cm^2) to give loadings ∼67.5 or ∼135 μg of the $Ni_{1-x}Fe_x$ catalysts, or drop coated onto ∼1 cm^2 area of Ni foam (Ni_{foam}; 1 × 3 cm^2) to give loadings of 135 μg of $Ni_{0.75}Fe_{0.25}$ catalyst. The ink was dried over 20 min at 60 °C and then left at room temperature for 20 min. Accuracy of the drop coating was checked by inductively coupled plasma mass spectrometry (ICP-MS) (∼97%) (Table S4). Homemade graphite clips were used for electrochemical measurements to avoid metal contamination.

The electrochemical experiments were performed with a Solartron SI 1287 Electrochemical Interface controlled by CorrWare for Windows Version 2-3d software. The reference electrode was a saturated calomel electrode (SCE; Fisher Scientific); however, all potentials in this paper are reported versus reversible hydrogen electrode (RHE). The measured potentials (E_{SCE}'s) were converted to an RHE scale according to

$$E_{RHE} = E_{SCE} + 0.059\text{pH} + 0.241 \quad (2)$$

$$\eta = E_{RHE} - 1.23\ \text{V} \quad (3)$$

where E_{RHE} is the potential versus reversible hydrogen electrode, E_{SCE} is the potential versus the saturated calomel electrode, and η is the overpotential. All electrochemistry experiments are performed in 1.0 M KOH solution (pH 13.6) at room temperature. The potential was calibrated by measuring against the homemade reversible hydrogen electrode potential using a Pt wire electrode under trapped hydrogen in the same electrolyte. Calibration was also done by measuring against Pt electrode in H_2-saturated 1.0 M KOH (Figure S18). A graphite rod formed the counter electrode. Uncompensated resistance (1 Ω) was estimated by ac impedance[28] and corrected for.

X-ray photoelectron spectroscopy (XPS) measurements were performed on a Kratos Axis 165 instrument. Brunauer−Emmett−Teller (BET) measurements were carried out using Autosorb Quantachrome 1MP. High resolution transmission electron microscopy (HRTEM) microscopy of the washed $Ni_{0.75}Fe_{0.25}$ HO-nps was performed at H-9500 with an accelerating voltage of 300 kV. Scanning transmission electron microscopy (STEM) was conducted at JEM2200FS with an accelerating voltage of 200 kV. Energy dispersive X-ray spectroscopy (EDS) was done under STEM mode. X-ray powder diffraction was performed on a X'Pert Pro MPD diffractometer (PANalitical, Netherlands) with a curved position-sensitive detector (CPS 120) and a Cu Kα1 radiation source operated at 40 kV and 20 mA with (l1/2 = 1.54060/1.54439 Å). Other detailed instrumentation information can be found in Supporting Information.

RESULTS AND DISCUSSION

Figure 1a shows the high resolution transmission electron microscopy images of the isolated, washed $Ni_{0.75}Fe_{0.25}$ HO-np

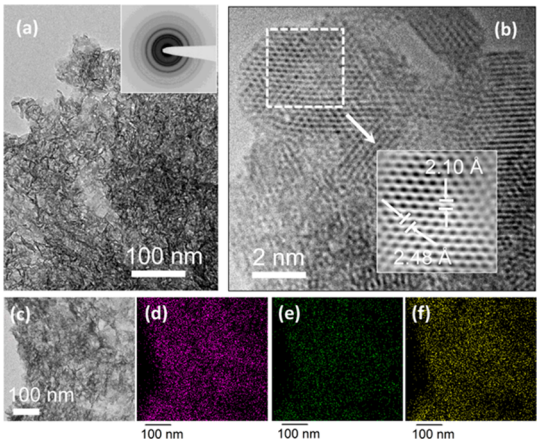

Figure 1. (a and b) High resolution transmission electron microscopy images of the isolated, washed $Ni_{0.75}Fe_{0.25}$ HO-nps. The inset of part a shows the selected area electron diffraction pattern. EDS elemental mappings for Ni (d), Fe (e), O (f), and the STEM image of the corresponding area (c).

catalyst. This is the most active mass-normalized WOR catalyst in the series prepared for this study (vide infra). The selected area electron diffraction pattern contains several rings (Figure 1a, inset), indicating regions with polycrystalline structure. Figure 1b shows that the catalyst consists mostly of regions with clear lattice images, indicating a largely polycrystalline $Ni_{0.75}Fe_{0.25}$ HO-np structure. The measured interplanar distances are 0.248 and 0.210 nm, corresponding to the (012) and (015) planes of α-$Ni(OH)_2$, respectively. A similar interplanar distance (0.25 nm) was reported by Dai et al. for the (012) lattice plane in their NiFe-LDH/CNT hybrid WOR catalyst.[14] The powder X-ray diffraction pattern of the isolated $Ni_{0.75}Fe_{0.25}$ HO-np also contained peaks corresponding to the (00n) planes of LDH structures, consistent with NiFe-LDH (JCPDS 51-0460) (Figure S19).[14,29−33] The Brunauer−Emmett−Teller (BET) surface area of the isolated, vacuum-dried $Ni_{0.75}Fe_{0.25}$ HO-np powder was 68.64 m^2 g^{-1}. The BET surface areas reported for other NiFe LDH materials in the literature range from 7 to 385 m^2 g^{-1}.[25,34−36]

The energy dispersive X-ray spectroscopy (EDS) elemental mapping indicates that the distribution of Ni, Fe, and O in the catalyst is uniform, with the ratio of Ni to Fe ∼ 3:1. The same ratio was measured by the ICP-MS after dissolving $Ni_{0.75}Fe_{0.25}$

DOI: 10.1021/acssuschemeng.6b02391
ACS Sustainable Chem. Eng. 2017, 5, 1106−1112

HO-nps in 0.1 M $HClO_4$, and by XPS (Table S4). Potassium and chloride ions were not detected by EDS or XPS in the isolated, washed catalyst (Figures S4 and S5). Thus, the initial ratio of Ni and Fe precursors is present in the isolated hydrous oxide nanoparticle product. Also, the absence of Cl^- shows that the anionic species in the LDH structure are oxides or hydroxides.

The XPS spectra (Figure S2) of the $Ni_{0.75}Fe_{0.25}$ HO-nps show that Fe is predominantly in the 3^+ oxidation state, resulting from air oxidation of Fe(II) during the synthesis.[37] We note that the use of $FeCl_3$ as precursor formed the catalyst with the same activity. Table S2 summarizes the key results with the Fe 2p signals at ~713 eV (Fe $2p_{3/2}$) and ~725 eV (Fe $2p_{1/2}$). Deconvolution of the O 1s signal at ~530−533 eV shows that the oxygen predominantly existed as OH^- incorporated into the lattice or on the surface, with only ~1% of lattice O^{2-} present (Figure S2).[20,38] The Ni XPS signals are consistent with $Ni(OH)_2$.[39] The detected presence of Fe(III) and OH^- and the likely presence of $Ni(OH)_2$ are also consistent with the Ni/Fe LDH catalyst structure.

The combined results from the characterization studies show that the $Ni_{0.75}Fe_{0.25}$ HO-nps predominantly exist as Ni/Fe LDH structures,[29,31] containing $Ni(II)(OH)_2$ and $Fe(III)(OH)_2^+$ octahedral centers in the hydroxide layers, with OH^- and H_2O intercalated between the layers. The overall equation for its formation would then be eq 4.

$$3Ni^{2+} + Fe^{2+} + 7.25OH^- + 0.25O_2 + 0.5H_2O \rightarrow 4[Ni_{0.75}Fe_{0.25}(OH)_2]^{0.25+}OH^-_{0.25} \quad (4)$$

Figure 2 shows the positive-going linear sweep voltammograms (LSVs) in 1 M KOH for a series of $Ni_{1-x}Fe_x$ HO-nps

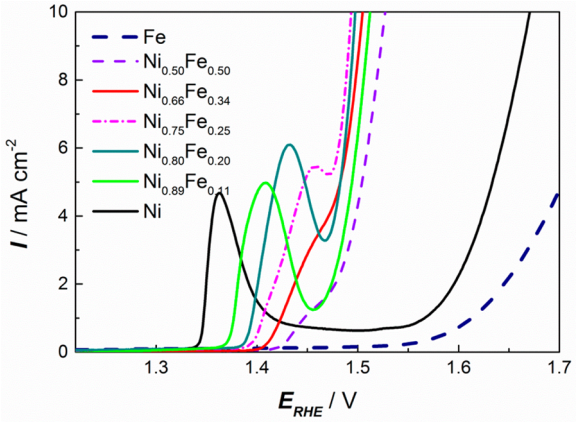

Figure 2. Voltammetric WOR over $Ni_{1-x}Fe_x$ HO-nps/CF in 1.0 M KOH from 1.2 to 1.7 V_{RHE} at 5 mV s^{-1}. All loadings of Ni + Fe = 0.0675 mg cm^{-2}.

deposited upon carbon fiber paper (CF). The total mass loading of Ni + Fe was the same (0.0675 mg cm^{-2}) for all the electrodes. The LSV of the Fe HO-np/CF is essentially featureless up to ~1.58 V_{RHE} (~350 mV overpotential), where the WOR current spikes up. The LSV of the Ni HO-np/CF contains a distinctive peak at 1.37 V_{RHE}, corresponding to the $Ni(OH)_2/Ni(O)OH$ redox couple.[40] This peak shifts to higher potentials when the mole fraction of Fe increased. Similar observations have been reported by others.[41−44] The shift to higher potentials may in part result from an increasing electron deficiency in the layered double hydroxide as Ni^{2+} is replaced by Fe^{3+} in the lattice. The WOR onset over the Ni HO-np/CF (x = 0) was ~1.56 V_{RHE} (~330 mV overpotential), which compares to the literature value after all traces of Fe were removed from the KOH.[43,45] The mixed systems are substantially more active than the pure Ni or Fe catalysts toward the WOR, with $Ni_{0.75}Fe_{0.25}$ HO-np/CF being the most active when normalized to the total mass of Ni + Fe. Table 2 summarizes the data. With increasing fractions of Fe, the onset potential decreased from 1.56 V_{RHE} over Ni HO-np/CF to 1.44 V_{RHE} (210 mV overpotential) over $Ni_{0.75}Fe_{0.25}$ HO-np/CF. The onset potential then increased to ~1.58 V_{RHE} over pure Fe HO-np/CF. The $Ni(O)OH/Ni(OH)_2$ peak in the cathodic sweeps of the LSVs did not overlap with the WOR, and could be used to estimate the number of electrochemically accessible Ni atoms in the samples. Table 2 lists the WOR overpotential for the HO-np at 6×10^4 A mol_{Ni}^{-1} in order to investigate the intrinsic activities of Ni within this series. The data show that the activity of Ni increases when the mole fraction of Fe (x) increases, even as x exceeds 0.25, the mole fraction within the most active mass-normalized WOR catalyst. Although this trend does not exclude other possibilities, it does suggest that the $Ni_{0.75}Fe_{0.25}$ HO-np is the most active catalyst by mass because the combination of Ni activation by Fe and the number of Ni atoms with the HO-np is optimized for the WOR. To our knowledge, this observation has not been reported previously.

The Tafel slopes for the Ni and Fe HO-np/CF were ~62 and 120 mV dec^{-1}, respectively. The slopes were substantially less over the most active catalysts $Ni_{0.75}Fe_{0.25}$ and $Ni_{0.80}Fe_{0.20}$ HO-np/CF (~29 and 30 mV dec^{-1}, respectively). The Tafel slopes were all near 40 mV dec^{-1} for the series of $Ni_{1-x}Fe_x$ HO-nps. As proposed by Gervasi et al., this Tafel slope is consistent (at low overvoltages and under steady-state conditions) with a mechanism with two net steps. The first is a reversible one-electron oxidation accompanied by coordination of hydroxide to a Ni(IV) active site (eq 5). The second is a turnover-limiting one-electron oxidation that occurs by reaction between dissolved hydroxide and $Ni(IV)(OH)_{ad}$ to generate O_2 (eq 6).[46,47] Equations 5 and 6 likely represent multistep processes. The turnover-limiting eq 6 likely resembles an attack by hydroxide on an electron-deficient oxygen species bonded to Ni(IV).

$$Ni(IV)_s + OH^- \rightleftharpoons Ni(IV)(OH)_{ad} + e^- \quad (5)$$

$$Ni(IV)(OH)_{ad} + OH^- \rightarrow Ni(IV)_s + \frac{1}{2}O_2 + H_2O + e^- \quad (6)$$

Cyclic voltammetry studies in the literature[44,48,49] and of our own indicate that the electron deficiency at Ni increases with the fraction of Fe in the lattice. Combining this observation with the mechanism proposed by Gervasi et al.,[47] we propose one way that Fe enhances eq 6 is by reducing the electron density at Ni, thereby increasing the reactivity of Ni-bound O-containing species toward attack by OH^-. This enhancement increases with the mole fraction of Fe in the HO-nps, but the mass activity of the catalyst also depends upon the mole fraction of Ni. Again, this proposal does not exclude other possibilities.

Table 2 also summarizes the LSV and galvanostatic WOR potentials of the series at 10 mA cm^{-2} (geometric). Again, the mixed catalyst $Ni_{0.75}Fe_{0.25}$ HO-np was the most active (E ~ 1.49−1.50 V_{RHE}, 260−270 mV overpotential) by mass of Ni + Fe.

DOI: 10.1021/acssuschemeng.6b02391
ACS Sustainable Chem. Eng. 2017, 5, 1106−1112

Table 2. Key Electrochemical Results for the $Ni_{1-x}Fe_x$ HO-np/CF and $Ni_{0.75}Fe_{0.25}$ HO-np/Ni_{foam} Electrodes[a]

	η_{onset}[b]/V_{RHE}		η at 10 mA cm^{-2}/V			
catalyst	LSV	Tafel	LSV	galv	η at 6 × 10^4 A mol_{Ni}^{-1}/V[c]	Tafel slope (mV dec^{-1})
Ni	0.33	0.31	0.44	0.45	0.47	62
$Ni_{0.89}Fe_{0.11}$	0.24	0.23	0.28	0.29	0.31	34
$Ni_{0.80}Fe_{0.20}$	0.22	0.23	0.27	0.27	0.29	30
$Ni_{0.75}Fe_{0.25}$	0.21	0.22	0.26	0.27	0.28	29
$Ni_{0.66}Fe_{0.34}$	0.23	0.22	0.27	0.28	0.26	34
$Ni_{0.50}Fe_{0.50}$	0.24	0.22	0.30	0.29	0.25	42
Fe	0.35	0.34	0.54	0.58	-	120
$Ni_{0.75}Fe_{0.25}$/Ni_{foam}[d]	0.19	0.20	0.23	0.24	0.28	24

[a]All loadings of Ni + Fe = 0.0675 mg cm^{-2}. [b]The onset overpotential was estimated by the intercept of the negative-going LSV with the *E* axis (Figures S7 and S8), and the beginning of the linear region in Tafel plots. (Figures S11 and S12). [c]The current density was chosen arbitrarily. The electrochemical accessible Ni normalized cyclic voltammograms are shown in Figures S9 and S10. [d]Catalyst loading on Ni foam Ni + Fe = 0.135 mg cm^{-2}.

The stability of the $Ni_{0.75}Fe_{0.25}$ HO-nps toward the WOR was investigated by galvanostatic and duty-cycle experiments. Figure 3 shows the 24 h galvanostatic WOR polarization curves over

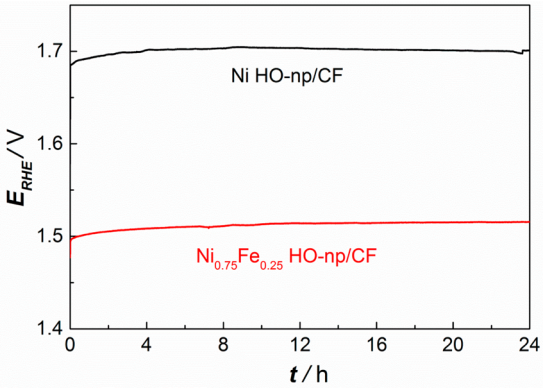

Figure 3. 24 h galvanostatic (10 mA cm^{-2}) WOR over Ni HO-np/CF and $Ni_{0.75}Fe_{0.25}$ HO-np/CF, loading Ni + Fe = 0.0675 mg cm^{-2}.

Ni and $Ni_{0.75}Fe_{0.25}$ HO-np/CF at j = 10 mA cm^{-2} with the loading Ni + Fe = 0.0675 mg cm^{-2}. Both catalysts displayed sustained polarization patterns during the entire galvanostatic water oxidation. The cyclic voltammograms (Figure S17) and XPS spectra (Figure S3) of the $Ni_{0.75}Fe_{0.25}$ HO-np/CF electrode were measured after the 24 h galvanostatic WOR. The area under the Ni(O)OH/$Ni(OH)_2$ cathodic peak (Figure S17) increased slightly (~4%), suggesting that no major restructuring of the catalyst occurred over the 24 h WOR. The Ni and Fe $2p_{3/2}$, $2p_{1/2}$ XPS peaks shifted by 0.5−1.0 eV to higher binding energies (Figure S3), and deconvolution of the O 1s peak showed that the amount of O^{2-} increased from <1% to ~3%. Taken together, the increases in the 2p binding energies and in the amount of O^{2-} suggest that the fraction of high oxidation state species, perhaps resembling Ni(O)OH, Fe(O)OH, increased over the 24 h WOR. This interpretation is tentative, however, because other factors, such as the degree of hydration, proportion of OH^- versus O^{2-} in the intercalated layers, etc., could also change over the 24 h WOR.

Strasser et al. developed duty-cycle tests that assess the durability of $IrNiO_x$ acidic WOR catalysts under conditions closer to an operating electrolyzer.[50] We applied similar duty-cycle tests to the $Ni_{0.75}Fe_{0.25}$ HO-np/CF for the WOR in base, except that we measured the WOR activity after each cycle at 10 mA cm^{-2}, rather than the reported 1 mA cm^{-2}. We utilized this harsher current density to be in keeping with the conventions of the alkaline WOR literature. Figure 4 shows

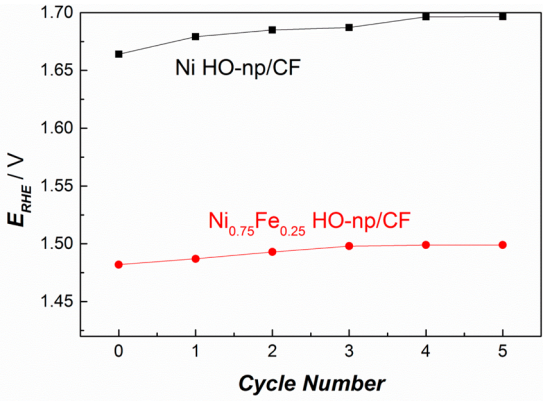

Figure 4. Voltammetric potential at 10 mA cm^{-2} vs duty cycle for Ni and $Ni_{0.75}Fe_{0.25}$ HO-np/CF, loading Ni + Fe = 0.0675 mg cm^{-2}.

plots of WOR potential at 10 mA cm^{-2} (E^{10}) versus number of duty cycles for Ni and $Ni_{0.75}Fe_{0.25}$ HO-np/CF. Both catalysts demonstrated high stabilities that are comparable to the acid $IrNiO_x$ systems reported by Strasser et al. Specifically, E^{10} increased by 30 mV, over 5 duty cycles with Ni HO-np/CF, and by only 17 mV, over 5 duty cycles with $Ni_{0.75}Fe_{0.25}$ HO-np/CF. Thus, the $Ni_{0.75}Fe_{0.25}$ HO-nps were robust to 24 h galvanostatic and duty-cycle tests.

The highest reported NiFe activities were obtained with NiFe LDH structures that were modified with oxidized graphene or carbon nanotubes, and supported on Ni foam at high loadings (0.25 to 1 mg cm^{-2}).[14,24,25] For comparison, we prepared electrodes with higher mass loadings of $Ni_{0.75}Fe_{0.25}$ HO-nps (Ni + Fe = 0.135 mg cm^{-2}) deposited on Ni foam and carbon fiber paper. Figure 5 compares the WOR LSVs of the $Ni_{0.75}Fe_{0.25}$ HO-np catalyst on Ni foam, on carbon fiber paper, and of bare Ni foam. The redox peaks and WOR activity of the bare Ni foam were negligible compared to the $Ni_{0.75}Fe_{0.25}$ HO-np deposit. The LSV overpotential at 10 mA cm^{-2} was only 234 mV (V_{RHE} = 1.46 V) over $Ni_{0.75}Fe_{0.25}$ HO-nps on Ni foam. This activity is comparable to the best, modified Ni−Fe catalysts in the literature (210 mV (0.25 mg cm^{-2})[25] and 224 mV (1 mg cm^{-2})[24]). The onset potential over $Ni_{0.75}Fe_{0.25}$ HO-np/Ni_{foam} was 1.42 V_{RHE} (190 mV overpotential), which also compares well to the lowest in the literature (180 mV).[16] The Tafel slope for the $Ni_{0.75}Fe_{0.25}$ HO-np/Ni_{foam} electrode was also low, 24

DOI: 10.1021/acssuschemeng.6b02391
ACS Sustainable Chem. Eng. 2017, 5, 1106−1112

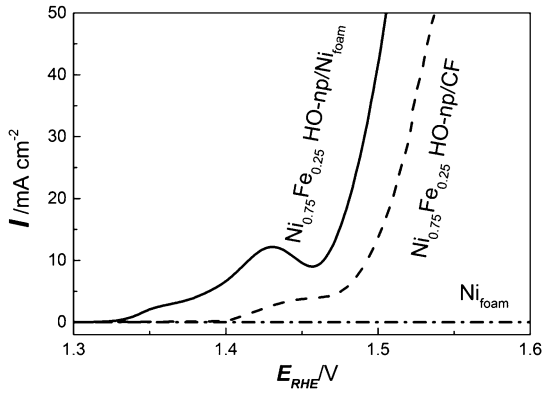

Figure 5. LSV WOR of $Ni_{0.75}Fe_{0.25}$ HO-nps on Ni foam (solid line, loading: Ni + Fe = 0.135 mg cm^{-2}), on carbon fiber paper (dash line, loading: Ni + Fe = 0.135 mg cm^{-2}) and bare Ni foam (dash dot line) in 1.0 M KOH at 5 mV s^{-1}.

mV dec^{-1}. The 24 h galvanostatic WOR at 10 mA cm^{-2} (Figure 6b, only ~1.47 V_{RHE}, 240 mV overpotential) and duty-cycle stability tests (Figure 6a, E^{10} increased by ~13 mV after 5 duty cycles) showed that the $Ni_{0.75}Fe_{0.25}$ HO-nps were more active (per gram Fe + Ni) and stable over Ni_{foam} than over carbon fiber paper. The charges under the $Ni(O)OH/Ni(OH)_2$ cathodic peak (Figure S8) showed that the utilization of Ni was ~11% in the $Ni_{0.75}Fe_{0.25}$ HO-np/CF electrode at 0.135 mg cm^{-2} mass loading Ni+ Fe. The utilization over Ni foam (48%) was substantially higher. When normalized to the electrochemically accessible sites estimated from the charges under the $Ni(O)OH/Ni(OH)_2$ cathodic peak (Figure S10), the $Ni_{0.75}Fe_{0.25}$ HO-nps possessed nearly the same WOR activity. Therefore, the increased activity can only come from the increased utilization of Ni (48%) when supported on Ni foam. More research is required to understand why the catalyst utilization is higher over Ni_{foam}. Regardless, these results show that the $Ni_{0.75}Fe_{0.25}$ HO-np/Ni_{foam} electrode, prepared in this simple manner, is comparable to the most active WOR catalysts reported to date.[51] The $Ni_{0.75}Fe_{0.25}$ HO-nps can also be isolated by centrifugation, washed with distilled water, and redispersed in distilled water by sonication. A control experiment showed that the isolated, washed, and dispersed $Ni_{0.75}Fe_{0.25}$ HO-nps had the same activity as the directly prepared catalyst (Figure S13).

This is one pot, open-air synthesis from simple Ni and Fe chlorides produced remarkably active and stable WOR catalysts. The synthesis is substrate-versatile and easily scaled. The hydrous oxide nanoparticles can be used directly from the reaction mixture, or isolated as a solid without loss in activity. We suggest that the presence of Fe decreases the electron density at Ni, which enhances the rate of reaction between Ni-oxide species and dissolved hydroxide in the turnover-limiting step. The simultaneous optimization of the activity of Ni by Fe, the fraction of Ni in the HO-nps, and the catalyst utilization contributed to the high activities and stabilities of these catalysts. Studies on incorporating the $Ni_{1-x}Fe_x$ HO-nps into prototype water electrolyzers, on the mechanism of the WOR over these catalysts,[13,30,32,39,45,49,52−63] and on support−catalyst interfaces are currently underway in our laboratories.

■ ASSOCIATED CONTENT

Supporting Information

The Supporting Information is available free of charge on the ACS Publications website at DOI: 10.1021/acssuschemeng.6b02391.

Detailed experimental procedure; XRD, XPS, ICP-MS, and cyclic voltammetry; and Tafel slope plots (PDF)

■ AUTHOR INFORMATION

Corresponding Author

*E-mail: sbergens@ualberta.ca.

Author Contributions

[§]The manuscript was written through contributions of all authors. All authors have given approval to the final version of the manuscript. C.W. and R.B.M. contributed equally.

Notes

The authors declare no competing financial interest.

■ ACKNOWLEDGMENTS

Authors thank Natural Sciences and Engineering Research Council of Canada (NSERC), Alberta Ingenuity: Technology Futures, and the University of Alberta for supporting this work. Authors thank Guangcheng Chen for ICP-MS measurements, Dimitre Karpuzov for XPS measurements, and Jian Chen for HR-TEM analysis.

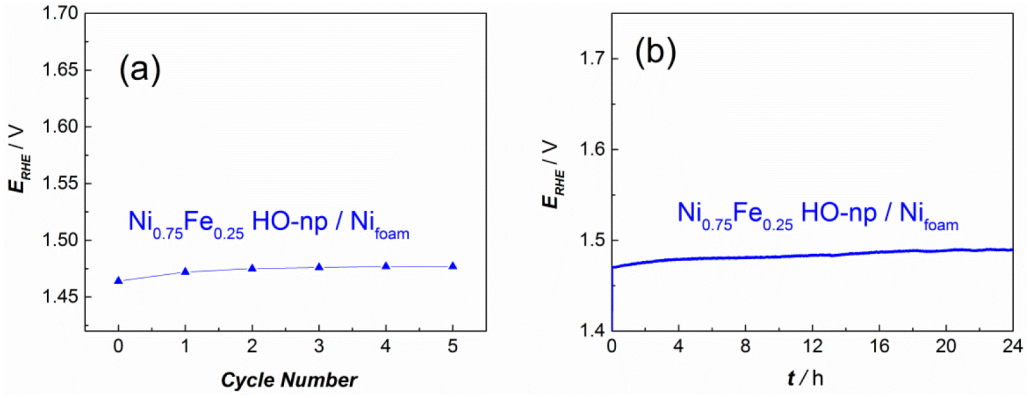

Figure 6. (a) Voltammetric potential at 10 mA cm^{-2} vs duty cycle and (b) 24 h galvanostatic (10 mA cm^{-2}) WOR over $Ni_{0.75}Fe_{0.25}$ HO-np/Ni_{foam} (loading Ni + Fe = 0.135 mg cm^{-2}).

DOI: 10.1021/acssuschemeng.6b02391
ACS Sustainable Chem. Eng. 2017, 5, 1106−1112

REFERENCES

(1) Acar, C.; Dincer, I. Impact assessment and efficiency evaluation of hydrogen production methods. *Int. J. Energy Res.* **2015**, *39*, 1757−1768.

(2) Nicoletti, G.; Arcuri, N.; Nicoletti, G.; Bruno, R. A technical and environmental comparison between hydrogen and some fossil fuels. *Energy Convers. Manage.* **2015**, *89*, 205−213.

(3) Verhelst, S. Recent progress in the use of hydrogen as a fuel for internal combustion engines. *Int. J. Hydrogen Energy* **2014**, *39*, 1071−1085.

(4) Dodds, P. E.; Staffell, I.; Hawkes, A. D.; Li, F.; Grünewald, P.; McDowall, W.; Ekins, P. Hydrogen and fuel cell technologies for heating: A review. *Int. J. Hydrogen Energy* **2015**, *40*, 2065−2083.

(5) Asadi, M.; Kim, K.; Liu, C.; Addepalli, A. V.; Abbasi, P.; Yasaei, P.; Phillips, P.; Behranginia, A.; Cerrato, J. M.; Haasch, R.; Zapol, P.; Kumar, B.; Klie, R. F.; Abiade, J.; Curtiss, L. A.; Salehi-Khojin, A. Nanostructured transition metal dichalcogenide electrocatalysts for CO2 reduction in ionic liquid. *Science* **2016**, *353*, 467−470.

(6) Carmo, M.; Fritz, D. L.; Mergel, J.; Stolten, D. A comprehensive review on PEM water electrolysis. *Int. J. Hydrogen Energy* **2013**, *38*, 4901−4934.

(7) Bodner, M.; Hofer, A.; Hacker, V. H2 generation from alkaline electrolyzer. *Wiley Interdiscip. Rev.: Energy Environ.* **2015**, *4*, 365−381.

(8) McCrory, C. C. L.; Jung, S.; Peters, J. C.; Jaramillo, T. F. Benchmarking Heterogeneous Electrocatalysts for the Oxygen Evolution Reaction. *J. Am. Chem. Soc.* **2013**, *135*, 16977−16987.

(9) McCrory, C. C. L.; Jung, S.; Ferrer, I. M.; Chatman, S. M.; Peters, J. C.; Jaramillo, T. F. Benchmarking Hydrogen Evolving Reaction and Oxygen Evolving Reaction Electrocatalysts for Solar Water Splitting Devices. *J. Am. Chem. Soc.* **2015**, *137*, 4347−4357.

(10) Jung, S.; McCrory, C. C. L.; Ferrer, I. M.; Peters, J. C.; Jaramillo, T. F. Benchmarking nanoparticulate metal oxide electrocatalysts for the alkaline water oxidation reaction. *J. Mater. Chem. A* **2016**, *4*, 3068−3076.

(11) Zeng, K.; Zhang, D. Recent progress in alkaline water electrolysis for hydrogen production and applications. *Prog. Energy Combust. Sci.* **2010**, *36*, 307−326.

(12) Marini, S.; Salvi, P.; Nelli, P.; Pesenti, R.; Villa, M.; Berrettoni, M.; Zangari, G.; Kiros, Y. Advanced alkaline water electrolysis. *Electrochim. Acta* **2012**, *82*, 384−391.

(13) Subbaraman, R.; Tripkovic, D.; Chang, K.-C.; Strmcnik, D.; Paulikas, A. P.; Hirunsit, P.; Chan, M.; Greeley, J.; Stamenkovic, V.; Markovic, N. M. Trends in activity for the water electrolyser reactions on 3d M(Ni,Co,Fe,Mn) hydr(oxy)oxide catalysts. *Nat. Mater.* **2012**, *11*, 550−557.

(14) Gong, M.; Li, Y.; Wang, H.; Liang, Y.; Wu, J. Z.; Zhou, J.; Wang, J.; Regier, T.; Wei, F.; Dai, H. An Advanced Ni−Fe Layered Double Hydroxide Electrocatalyst for Water Oxidation. *J. Am. Chem. Soc.* **2013**, *135*, 8452−8455.

(15) Smith, R. D. L.; Prevot, M. S.; Fagan, R. D.; Trudel, S.; Berlinguette, C. P. Water Oxidation Catalysis: Electrocatalytic Response to Metal Stoichiometry in Amorphous Metal Oxide Films Containing Iron, Cobalt, and Nickel. *J. Am. Chem. Soc.* **2013**, *135*, 11580−11586.

(16) Smith, R. D. L.; Prévot, M. S.; Fagan, R. D.; Zhang, Z.; Sedach, P. A.; Siu, M. K. J.; Trudel, S.; Berlinguette, C. P. Photochemical Route for Accessing Amorphous Metal Oxide Materials for Water Oxidation Catalysis. *Science* **2013**, *340*, 60−63.

(17) Trotochaud, L.; Young, S. L.; Ranney, J. K.; Boettcher, S. W. Nickel−Iron Oxyhydroxide Oxygen-Evolution Electrocatalysts: The Role of Intentional and Incidental Iron Incorporation. *J. Am. Chem. Soc.* **2014**, *136*, 6744−6753.

(18) Fabbri, E.; Habereder, A.; Waltar, K.; Kotz, R.; Schmidt, T. J. Developments and perspectives of oxide-based catalysts for the oxygen evolution reaction. *Catal. Sci. Technol.* **2014**, *4*, 3800−3821.

(19) Swierk, J. R.; Klaus, S.; Trotochaud, L.; Bell, A. T.; Tilley, T. D. Electrochemical Study of the Energetics of the Oxygen Evolution Reaction at Nickel Iron (Oxy)Hydroxide Catalysts. *J. Phys. Chem. C* **2015**, *119*, 19022−19029.

(20) Zhao, Z.; Wu, H.; He, H.; Xu, X.; Jin, Y. Self-standing non-noble metal (Ni-Fe) oxide nanotube array anode catalysts with synergistic reactivity for high-performance water oxidation. *J. Mater. Chem. A* **2015**, *3*, 7179−7186.

(21) Zhang, D.; Meng, L.; Shi, J.; Wang, N.; Liu, S.; Li, C. One-step preparation of optically transparent Ni-Fe oxide film electrocatalyst for oxygen evolution reaction. *Electrochim. Acta* **2015**, *169*, 402−408.

(22) Gong, M.; Dai, H. A mini review of NiFe-based materials as highly active oxygen evolution reaction electrocatalysts. *Nano Res.* **2015**, *8*, 23−39.

(23) Merrill, M. D.; Dougherty, R. C. Metal Oxide Catalysts for the Evolution of O2 from H2O. *J. Phys. Chem. C* **2008**, *112*, 3655−3666.

(24) Li, Z.; Shao, M.; An, H.; Wang, Z.; Xu, S.; Wei, M.; Evans, D. G.; Duan, X. Fast electrosynthesis of Fe-containing layered double hydroxide arrays toward highly efficient electrocatalytic oxidation reactions. *Chem. Sci.* **2015**, *6*, 6624−6631.

(25) Long, X.; Li, J.; Xiao, S.; Yan, K.; Wang, Z.; Chen, H.; Yang, S. A strongly coupled graphene and FeNi double hydroxide hybrid as an excellent electrocatalyst for the oxygen evolution reaction. *Angew. Chem., Int. Ed.* **2014**, *53*, 7584−7588.

(26) Zhang, B.; Zheng, X.; Voznyy, O.; Comin, R.; Bajdich, M.; García-Melchor, M.; Han, L.; Xu, J.; Liu, M.; Zheng, L.; García de Arquer, F. P.; Dinh, C. T.; Fan, F.; Yuan, M.; Yassitepe, E.; Chen, N.; Regier, T.; Liu, P.; Li, Y.; De Luna, P.; Janmohamed, A.; Xin, H. L.; Yang, H.; Vojvodic, A.; Sargent, E. H. Homogeneously dispersed multimetal oxygen-evolving catalysts. *Science* **2016**, *352*, 333−337.

(27) Moghaddam, R. B.; Wang, C.; Sorge, J. B.; Brett, M. J.; Bergens, S. H. Easily prepared, high activity Ir-Ni oxide catalysts for water oxidation. *Electrochem. Commun.* **2015**, *60*, 109−112.

(28) Gao, M.; Sheng, W.; Zhuang, Z.; Fang, Q.; Gu, S.; Jiang, J.; Yan, Y. Efficient water oxidation using nanostructured alpha-nickel-hydroxide as an electrocatalyst. *J. Am. Chem. Soc.* **2014**, *136*, 7077−7084.

(29) Khan, A. I.; O'Hare, D. Intercalation chemistry of layered double hydroxides: recent developments and applications. *J. Mater. Chem.* **2002**, *12*, 3191−3198.

(30) Oliver-Tolentino, M. A.; Vazquez-Samperio, J.; Manzo-Robledo, A.; Gonzalez-Huerta, R. D.; Flores-Moreno, J. L.; Ramirez-Rosales, D.; Guzman-Vargas, A. An Approach to Understanding the Electrocatalytic Activity Enhancement by Superexchange Interaction toward OER in Alkaline Media of Ni-Fe LDH. *J. Phys. Chem. C* **2014**, *118*, 22432−22438.

(31) Song, F.; Hu, X. Exfoliation of layered double hydroxides for enhanced oxygen evolution catalysis. *Nat. Commun.* **2014**, *5*, 4477.

(32) Friebel, D.; Louie, M. W.; Bajdich, M.; Sanwald, K. E.; Cai, Y.; Wise, A. M.; Cheng, M.-J.; Sokaras, D.; Weng, T.-C.; Alonso-Mori, R.; Davis, R. C.; Bargar, J. R.; Nørskov, J. K.; Nilsson, A.; Bell, A. T. Identification of Highly Active Fe Sites in (Ni,Fe)OOH for Electrocatalytic Water Splitting. *J. Am. Chem. Soc.* **2015**, *137*, 1305−1313.

(33) Lu, Z.; Qian, L.; Tian, Y.; Li, Y.; Sun, X.; Duan, X. Ternary NiFeMn layered double hydroxides as highly-efficient oxygen evolution catalysts. *Chem. Commun.* **2016**, *52*, 908−911.

(34) Saiah, F. B. D.; Su, B.-L.; Bettahar, N. Nickel−iron layered double hydroxide (LDH): Textural properties upon hydrothermal treatments and application on dye sorption. *J. Hazard. Mater.* **2009**, *165*, 206−217.

(35) Zhou, L.-J.; Huang, X.; Chen, H.; Jin, P.; Li, G.-D.; Zou, X. A high surface area flower-like Ni-Fe layered double hydroxide for electrocatalytic water oxidation reaction. *Dalton Transactions* **2015**, *44*, 11592−11600.

(36) Ruano-Casero, R. J.; Pérez-Bernal, M. E.; Rives, V. Preparation and Properties of Nickel and Iron Oxides obtained by Calcination of Layered Double Hydroxides. *Z. Anorg. Allg. Chem.* **2005**, *631*, 2142−2150.

(37) Grosvenor, A. P.; Kobe, B. A.; Biesinger, M. C.; McIntyre, N. S. Investigation of multiplet splitting of Fe 2p XPS spectra and bonding in iron compounds. *Surf. Interface Anal.* **2004**, *36*, 1564−1574.

DOI: 10.1021/acssuschemeng.6b02391
ACS Sustainable Chem. Eng. 2017, 5, 1106−1112

(38) Dupin, J.-C.; Gonbeau, D.; Vinatier, P.; Levasseur, A. Systematic XPS studies of metal oxides, hydroxides and peroxides. *Phys. Chem. Chem. Phys.* **2000**, *2*, 1319−1324.
(39) Ali-Löytty, H.; Louie, M. W.; Singh, M. R.; Li, L.; Sanchez Casalongue, H. G.; Ogasawara, H.; Crumlin, E. J.; Liu, Z.; Bell, A. T.; Nilsson, A.; Friebel, D. Ambient-Pressure XPS Study of a Ni−Fe Electrocatalyst for the Oxygen Evolution Reaction. *J. Phys. Chem. C* **2016**, *120*, 2247−2253.
(40) Kim, M. S.; Kim, K. B. A Study on the Phase Transformation of Electrochemically Precipitated Nickel Hydroxides Using an Electrochemical Quartz Crystal Microbalance. *J. Electrochem. Soc.* **1998**, *145*, 507−511.
(41) Corrigan, D. A. The Catalysis of the Oxygen Evolution Reaction by Iron Impurities in Thin Film Nickel Oxide Electrodes. *J. Electrochem. Soc.* **1987**, *134*, 377−384.
(42) Li, X.; Walsh, F. C.; Pletcher, D. Nickel based electrocatalysts for oxygen evolution in high current density, alkaline water electrolysers. *Phys. Chem. Chem. Phys.* **2011**, *13*, 1162−1167.
(43) Trotochaud, L.; Young, S. L.; Ranney, J. K.; Boettcher, S. W. Nickel-iron oxyhydroxide oxygen-evolution electrocatalysts: the role of intentional and incidental iron incorporation. *J. Am. Chem. Soc.* **2014**, *136*, 6744−6753.
(44) Bates, M. K.; Jia, Q.; Doan, H.; Liang, W.; Mukerjee, S. Charge-Transfer Effects in Ni−Fe and Ni−Fe−Co Mixed-Metal Oxides for the Alkaline Oxygen Evolution Reaction. *ACS Catal.* **2016**, *6*, 155−161.
(45) Zou, S. H.; Burke, M. S.; Kast, M. G.; Fan, J.; Danilovic, N.; Boettcher, S. W. Fe (Oxy)hydroxide Oxygen Evolution Reaction Electrocatalysis: Intrinsic Activity and the Roles of Electrical Conductivity, Substrate, and Dissolution. *Chem. Mater.* **2015**, *27*, 8011−8020.
(46) Lu, Z.; Xu, W.; Zhu, W.; Yang, Q.; Lei, X.; Liu, J.; Li, Y.; Sun, X.; Duan, X. Three-dimensional NiFe layered double hydroxide film for high-efficiency oxygen evolution reaction. *Chem. Commun.* **2014**, *50*, 6479−6482.
(47) Castro, E. B.; Gervasi, C. A. Electrodeposited Ni−Co-oxide electrodes:characterization and kinetics of the oxygen evolution reaction. *Int. J. Hydrogen Energy* **2000**, *25*, 1163−1170.
(48) Louie, M. W.; Bell, A. T. An investigation of thin-film Ni-Fe oxide catalysts for the electrochemical evolution of oxygen. *J. Am. Chem. Soc.* **2013**, *135*, 12329−37.
(49) Yeo, B. S.; Bell, A. T. In Situ Raman Study of Nickel Oxide and Gold-Supported Nickel Oxide Catalysts for the Electrochemical Evolution of Oxygen. *J. Phys. Chem. C* **2012**, *116*, 8394−8400.
(50) Nong, H. N.; Oh, H.-S.; Reier, T.; Willinger, E.; Willinger, M.-G.; Petkov, V.; Teschner, D.; Strasser, P. Oxide-Supported IrNiOx Core−Shell Particles as Efficient, Cost-Effective, and Stable Catalysts for Electrochemical Water Splitting. *Angew. Chem., Int. Ed.* **2015**, *54*, 2975−2979.
(51) Precise comparisons with the literature are difficult because the experimental parameters, *iR* compensation, criteria for onset potentials, and errors in electrode geometries vary among the reports.
(52) Guerlou-Demourgues, L.; Fournès, L.; Delmas, C. In Situ 57Fe Mössbauer Spectroscopy Study of the Electrochemical Behavior of an Iron-Substituted Nickel Hydroxide Electrode. *J. Electrochem. Soc.* **1996**, *143*, 3083−3088.
(53) Balasubramanian, M.; Melendres, C. A.; Mini, S. X-ray Absorption Spectroscopy Studies of the Local Atomic and Electronic Structure of Iron Incorporated into Electrodeposited Hydrous Nickel Oxide Films†. *J. Phys. Chem. B* **2000**, *104*, 4300−4306.
(54) Bediako, D. K.; Lassalle-Kaiser, B.; Surendranath, Y.; Yano, J.; Yachandra, V. K.; Nocera, D. G. Structure−Activity Correlations in a Nickel−Borate Oxygen Evolution Catalyst. *J. Am. Chem. Soc.* **2012**, *134*, 6801−6809.
(55) Landon, J.; Demeter, E.; İnoğlu, N.; Keturakis, C.; Wachs, I. E.; Vasić, R.; Frenkel, A. I.; Kitchin, J. R. Spectroscopic Characterization of Mixed Fe−Ni Oxide Electrocatalysts for the Oxygen Evolution Reaction in Alkaline Electrolytes. *ACS Catal.* **2012**, *2*, 1793−1801.
(56) Bediako, D. K.; Surendranath, Y.; Nocera, D. G. Mechanistic Studies of the Oxygen Evolution Reaction Mediated by a Nickel−Borate Thin Film Electrocatalyst. *J. Am. Chem. Soc.* **2013**, *135*, 3662−3674.
(57) Louie, M. W.; Bell, A. T. An Investigation of Thin-Film Ni−Fe Oxide Catalysts for the Electrochemical Evolution of Oxygen. *J. Am. Chem. Soc.* **2013**, *135*, 12329−12337.
(58) Marrani, A. G.; Novelli, V.; Sheehan, S.; Dowling, D. P.; Dini, D. Probing the Redox States at the Surface of Electroactive Nanoporous NiO Thin Films. *ACS Appl. Mater. Interfaces* **2014**, *6*, 143−152.
(59) Chen, J. Y. C.; Dang, L. N.; Liang, H. F.; Bi, W. L.; Gerken, J. B.; Jin, S.; Alp, E. E.; Stahl, S. S. Operando Analysis of NiFe and Fe Oxyhydroxide Electrocatalysts for Water Oxidation: Detection of Fe4+ by Mossbauer Spectroscopy. *J. Am. Chem. Soc.* **2015**, *137*, 15090−15093.
(60) Trześniewski, B. J.; Diaz-Morales, O.; Vermaas, D. A.; Longo, A.; Bras, W.; Koper, M. T. M.; Smith, W. A. In Situ Observation of Active Oxygen Species in Fe-Containing Ni-Based Oxygen Evolution Catalysts: The Effect of pH on Electrochemical Activity. *J. Am. Chem. Soc.* **2015**, *137*, 15112−15121.
(61) Klaus, S.; Cai, Y.; Louie, M. W.; Trotochaud, L.; Bell, A. T. Effects of Fe Electrolyte Impurities on Ni(OH)2/NiOOH Structure and Oxygen Evolution Activity. *J. Phys. Chem. C* **2015**, *119*, 7243−7254.
(62) Wang, D.; Zhou, J.; Hu, Y.; Yang, J.; Han, N.; Li, Y.; Sham, T.-K. In Situ X-ray Absorption Near-Edge Structure Study of Advanced NiFe(OH)x Electrocatalyst on Carbon Paper for Water Oxidation. *J. Phys. Chem. C* **2015**, *119*, 19573−19583.
(63) Rong, X.; Parolin, J.; Kolpak, A. M. A Fundamental Relationship between Reaction Mechanism and Stability in Metal Oxide Catalysts for Oxygen Evolution. *ACS Catal.* **2016**, *6*, 1153−1158.

DOI: 10.1021/acssuschemeng.6b02391
ACS Sustainable Chem. Eng. 2017, 5, 1106−1112